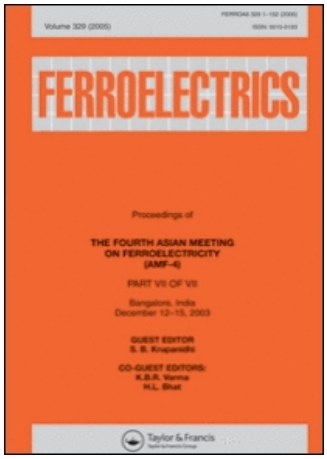

Ferroelectrics
Publication details, including instructions for authors and subscription information:
http://www.informaworld.com/smpp/title~content=t713617887

Epitaxial Multiferroic $BiFeO_3$ Thin Films: Progress and Future Directions

Y. H. Chu [a]; L. W. Martin [a]; Q. Zhan [a]; P. L. Yang [a]; M. P. Cruz **[a]; K. Lee [a]; M. Barry [a]; S. Y. Yang [a]; R. Ramesh [a]
[a] Department of Materials Science and Engineering & Department of Physics, University of California, Berkeley, CA

First Published on: 01 January 2007
To cite this Article: Chu, Y. H., Martin, L. W., Zhan, Q., Yang, P. L., Cruz **, M. P., Lee, K., Barry, M., Yang, S. Y. and Ramesh, R. (2007) 'Epitaxial Multiferroic $BiFeO_3$ Thin Films: Progress and Future Directions', Ferroelectrics, 354:1, 167 - 177
To link to this article: DOI: 10.1080/00150190701454867
URL: http://dx.doi.org/10.1080/00150190701454867

Ferroelectrics, 354:167–177, 2007

ISSN: 0015-0193 print / 1521-0464 online
DOI: 10.1080/00150190701454867

Epitaxial Multiferroic $BiFeO_3$ Thin Films: Progress and Future Directions

Y. H. CHU,* L. W. MARTIN, Q. ZHAN, P. L. YANG, M. P. CRUZ,** K. LEE, M. BARRY, S. Y. YANG, AND R. RAMESH

Department of Materials Science and Engineering & Department of Physics, University of California, Berkeley, CA 94720

We write this article in honor of Professor Vitaly L. Ginzburg, truly the father of the field of ferroelectricity. This article serves as a review of the current state of research pertaining to multiferroic $BiFeO_3$ thin films. In this review we will delve into details of the growth of $BiFeO_3$ thin films and the use of piezoforce microscopy and x-ray reciprocal space mapping to characterize the crystal structure and domain structure of $BiFeO_3$. We will also discuss the use of vicinal and asymmetric substrates to simplify the domain structure in $BiFeO_3$. By simplifying the domain structure we can, in turn, control the ferroelectric switching mechanisms in $BiFeO_3$. Finally we describe the basic ferroelectric properties of BFO films and discuss the critical issues needed to be solved in $BiFeO_3$ films including leakage, complex domain structure, coercivity, and reliability. Such results are promising for continued exploration for detailed multiferroic-coupling studies in the magnetoelectric $BiFeO_3$ system and $BiFeO_3$, in turn, provides a model platform with which to realize the exciting possibility of electrically control magnetism.

Keywords Bismuth ferrite; multiferroics; domain structure; heteroepitaxy

I. Introduction

It is a pleasure and an honor to be able to contribute to this special issue, which celebrates the 90th birthday of Professor Ginzburg. Anyone who has entered and flourished in the field of ferroelectricity and ferroic materials in general, is a student of Professor Ginzburg. His work [1] with Landau (and Devonshire, LGD model) obviously laid the foundation for several generations of materials physicists to understand this complicated physical phenomenon and the accompanying rich diversity of materials responses. The GLGD model is also the starting point to understand even more complicated coupling phenomena, such as those that exist in multiferroic materials. Such materials exhibit the co-existence of multiple order parameters (for example, ferroelectricity and antiferromagnetism). Magnetoelectric effects in multiferroic materials have attracted much attention because of the intriguing science underpinning this phenomenon. Magnetoelectric coupling between the electric and magnetic

Received in final form March 25, 2007.
*Corresponding author. E-mail: yhchu@berkeley.edu
**The current address of this author is Universidad Nacional Autónoma de México. Centro de Ciencias de la Materia Condensada. Km 107 Caretera Tijuana-Ensenada. Ensenada, B.C., Mexico. C.P. 22800.

order parameters has been theoretically predicted [2], and there is currently intense interest in the implementation of this coupling in a device architecture that can take advantage of these properties [3–7]. Single phase multiferroics, materials which simultaneously show magnetization and polarization at ambient conditions, however, remain elusive as most multiferroic systems exhibit the coexistence of multiple order parameters only at low temperatures [8, 9]. Multiferroics can be alternatively be synthesized as a composite system, e.g. as a product property of a composite phase of a magnetostrictive and a piezoelectric material [10, 11]. Hence, much experimental effort has been spent investigating new single phase and composite multiferroics as it is very difficult to create single phase multiferroic materials that exhibit room temperature multiferroicity.

One exception to this is $BiFeO_3$ (BFO). BFO is a room temperature, single-phase, multiferroic material with a high ferroelectric Curie temperature ($\sim$1103 K) [12] and a high antiferromagnetic Néel temperature ($\sim$643 K) [13]. The structure of BFO is characterized by two distorted perovskite unit cells ($a_r = 3.96$ Å, $\alpha_r = 0.6^\circ$) connected along their body diagonal, denoted as the pseudocubic $\langle 111 \rangle$, to build the rhombohedral unit cell [14]. The ferroelectric state is realized by a large displacement of the Bi ions relative to the FeO_6 octahedra. The ferroelectric polarization in BFO, therefore, can have directions along the four cube diagonals ($\langle 111 \rangle$), and the direction of the polarization can be changed by ferroelectric (180°) and ferroelastic switching events (71° and 109°) [15]. The antiferromagnetic ordering of BFO is G-type, hence the Fe magnetic moments are aligned ferromagnetically within pseudocubic (111) planes and antiferromagnetically between adjacent (111) planes. The preferred orientation of the antiferromagnetically aligned spins is in the (111) plane perpendicular to the ferroelectric polarization direction, with six equivalent easy axes within that plane [16]. The antiferromagnetism is therefore coupled to the ferroelectric polarization. Recent studies of BFO thin films have shown the existence of a large ferroelectric polarization, as well as a small net magnetization of the Dzyaloshinskii-Moriya type resulting from a canting of the antiferromagnetic sublattice [16, 17]. Moreover, the coupling between ferroelectricity and antiferromagnetism in BFO thin films was also demonstrated by using a combined technique of piezoforce microscopy (PFM) and photoemission electron microscopy (PEEM), which is attributed to the coupling of both antiferromagnetic and ferroelectric domains to the underlying domain switching events [18]. Ferroelastic switching of the polarization changes the rhombohedral axis of the system and is therefore accompanied by a switching of the ferroelastic domain state, which in turn changes the orientation of the easy magnetization plane.

It has also been noted, however, that BFO films show a very complicated domain structure, which needs to be understood for eventual device integration. In addition, at normal operating temperatures for devices, the ferroelectric nature of BFO could dominate the magnetic nature of the system due to the relative robustness of the ferroelectric order parameter; therefore, controlling the ferroelectric domain structure becomes a critical issue for device functionality. Moreover, with an ever-expanding demand for data storage, transducers and microelectromechanical systems (MEMS) applications, materials with superior ferroelectric and piezoelectric responses are of great interest. The lead zirconate titanate (PZT) family of materials, to this point, has served as the cornerstone for such applications. A critical drawback of this material, however, is its toxicity due to the lead content. In February 2003, this was made very clear as the European Union adopted the Restriction of Hazardous Substances Directive which has hence taken effect as of July 1, 2006. Although the initial directive focused on open components of devices, the message is nonetheless clear: highly toxic elements like lead will eventually be phased out of devices. Because of this, lead-free ferroelectrics, BFO especially because of its superior ferroelectric properties,

have attracted a great deal of attention [19, 20]. In the remainder of this review we will review the major findings concerning the growth of BFO thin films, control of the domain structures in these films, and the ferroelectricity and other properties of BFO thin films.

II. Progress

A veritable plethora of research has been done on the growth and characterization of epitaxial films because of the role and influence of heteroepitaxial constraint. Theoretical predictions for heteroepitaxial constrained ferroelectric and magnetic properties can be carried out via first-principles calculations [21, 22]. Such theoretical treatments point to the ferroelectric polarization in multiferroic BFO being almost entirely insensitive to strain. The effect, however, of a small monoclinic distortion arising from strain on BFO may lead to a break in the magnetic symmetry and correspondingly may lead to the formation of a preferred antiferromagnetic axis [20]. This is important because in this case we would expect the antiferromagnetic axis to rotate by 90° for a ferroelectric 109° change in polarization and to be preserved during a 71° switching event. This implies that an added level of control might exist in the realm of magnetoelectric coupling.

In light of these theoretical calculations, a great many experiments have been under taken to explore the ferroelectric, magnetic, and magnetoelectric nature of epitaxial BFO thin films. High quality epitaxial BFO films have been prepared by pulsed laser deposition (PLD) [6, 23], radio-frequency (RF) sputtering [24, 25], metalorganic chemical vapor deposition (MOCVD) [20, 26], and chemical solution deposition (CSD) on various substrates [27], including $SrTiO_3$ (STO), $DyScO_3$ (DSO), and $LaAlO_3$. In order to probe the ferroelectric nature of these films, BFO films have typically been grown on various conducting oxide bottom electrodes including $SrRuO_3$ (SRO), $(La,Sr)MnO_3$, and $LaNiO_3$. In a number of studies, the crystallinity of the films and a measure of the overall quality of the film has been probed via X-ray diffraction (XRD). Figure 1(a) shows typical 2θ X-ray diffraction results for the heterostructures. BFO films grown on DSO substrates show very narrow rocking curve scans pointing to the extremely high quality and epitaxial nature of these films (Fig. 1(b)). Additionally, at these thicknesses, the BFO films appear to be relaxed to a derivative of the bulk rhombohedral structure as can be seen from the φ-scan of the rhombohedrally nondegenerate 210_R reflection in BFO (Fig. 1(c)). However, an additional slight monoclinic distortion to the lattice could exist. The quality of the heterostructures can additionally be probed using transmission electron microscopy (TEM) with which we can identify the presence of a highly coherent and smooth interface between BFO and the electrode layer. Figure 1(d) is high resolution TEM (HRTEM) image of the interfaces between SRO and BFO in a symmetric device structure prepared by the PLD process. The HRTEM image shows the perfect epitaxy and clear interface between the BFO and SRO layers.

To understand the effect of strain on the structure of epitaxial BFO films, high-resolution XRD (HRXRD) measurements are generaly performed. Reciprocal space mapping (RSM) by synchrotron x-ray source is further used to identify the crystal structure of epitaxial BFO films [28, 29]. For BFO films on a STO substrate the BFO lattice is isotropically compressed in the plane of the film and therefore elongated in the out-of-plane direction because of the lattice mismatch between STO ($a = 3.905$ Å) and BFO (3.96 Å). Such an effect can lead to the formation of a monoclinically distorted structure for BFO films on STO (001) and (110) substrates. Based on this model the structural variants of a BFO thin film can also be characterized by detailed RSM measurements [30].

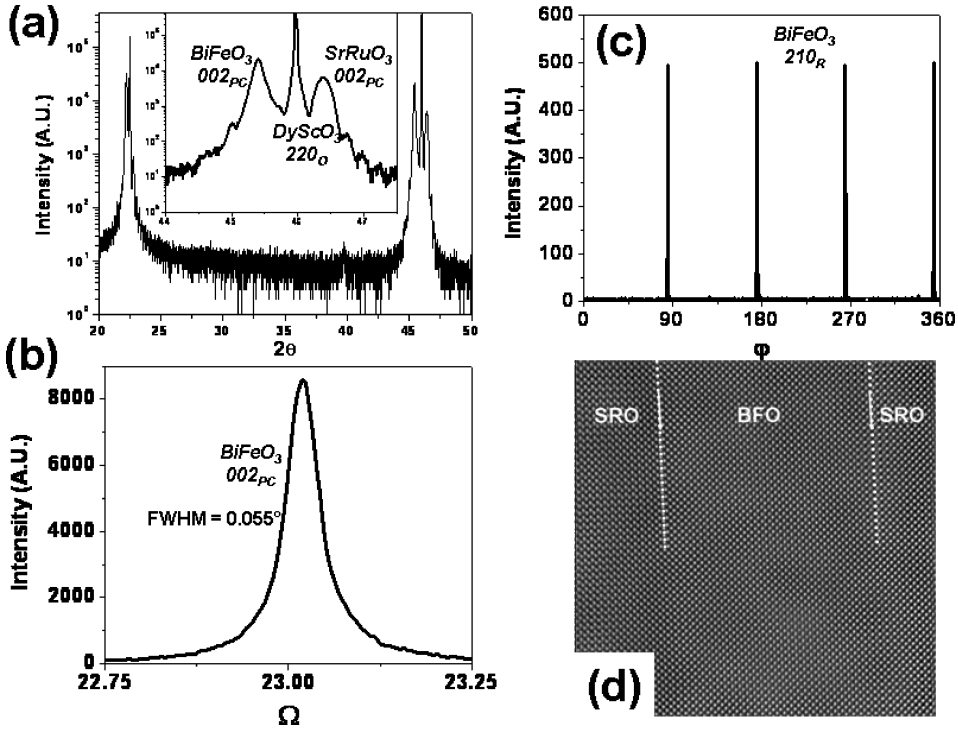

Figure 1. X-ray diffraction showing (a) wide θ–2θ scan of a (001) BFO/SRO/DSO film, inset shows a zoom in on the 002 peaks, (b) a rocking curve of BFO 002PC peak with a FWHM of 0.055°, (c), a phi scan of the BFO 210R peak, and (d) HRTEM image of SRO/BFO/SRO/STO heterostructure.

The ferroelectric domain structure of an epitaxial BFO film with different orientations and different strain states can be modeled using the phase-field method [31] in which the spatial distribution of the polarization field and its evolution is described by the time dependent Ginzburg-Landau (TDGL) equations [32]. The domain wall energy, electrostatic energy, and elastic energy contributions to the total energy are incorporated to complete the analysis. A short-circuit electrostatic boundary condition is assumed on both the top surface and the film/electrode interface. These models can provide great insight into the equilibrium domain structure for BFO thin films and can help experimentalists engineer and understand the factors important for simplifying that domain structure.

For a BFO film grown on a (001)-oriented perovskite substrate, there are eight possible ferroelectric polarization directions corresponding to the four structural variants of the rhombohedral phase. Domain patterns can develop with either {100} or {101} boundaries for (001) oriented rhombohedral films [33]. In both cases, the individual domains in the patterns are energetically degenerate and thus equal width stripe patterns are theoretically predicted. When the spontaneous polarization is included in the analysis, the {100} boundary patterns have no normal component of the net polarization, whereas the {101} boundary patterns correspond to the fully poled state. The formation of domain patterns leads to the release of elastic energy at the expense of increased interfacial energy associated with the domain boundaries. In the case of a film on a STO (110) substrate the smaller substrate lattice parameter which compressively strains the BFO film causes the structure to favor four of the eight polarization variants. Since they have exactly the same spontaneous deformation

on the (110) plane, the twin-structure formed by those variant pairs does not change the magnitude of the elastic energy; therefore, these twin boundaries are thermodynamically unstable and are not expected to exist in films grown on STO (110) substrates. Finally for growth on a STO (111) substrate, the polarization variants perpendicular to the film surface have the lowest energy for films grown under compressive strain. The stable domain structure in this case, therefore, is a single domain with a downward directed polarization.

Experimentally, the domain structures of BFO thin films on STO substrates are revealed and characterized by PFM [30, 34]. In PFM, domains with up and down polarizations give rise to opposite contrast in out-of-plane (OP)-PFM images and in-plane components of polarization produce a torque on the imaging cantilever and create contrast in the in-plane (IP)-PFM images. More specifically, domains with polarization vectors along the scanning cantilever's long axis do not give rise to any IP-PFM contrast for they do not produce any torque on the cantilever. In contrast, domains with polarization pointing to the right with respect to the cantilever's long axis should produce an opposite tone as compared with domains having polarization pointing to the left of the cantilever. The reason for this is the antiphase IP-peizoresponse (PR) signals produced by these domains. Therefore, by combining the OP-PFM and IP-PFM images, we can identify the polarization direction of each domain. Figure 2(a) shows an IP-PFM image of a BFO film grown on a (001) STO substrate. The three contrast levels observed in the IP-PFM images acquired along the two orthogonal ⟨110⟩ directions, together with the uniform OP-PFM contrast (not shown), indicate that the domain structure of the BFO films is characterized by four polarization variants. The twin-wall orientations for stripe-like domains match well with those predicted from the phase-field simulation. Figure 2(b) shows the ferroelectric domain structure of BFO films grown on STO (110) substrates, (imaged with the cantilever along [1–10]), exhibiting only two ferroelectric variants with net polarization pointing down over large areas. We have verified the domain structure of the BFO films grown on STO (111) substrates and, as anticipated, these films exhibited only one contrast in the out-of-plane (OP) (not shown) PFM image and no contrast for IP PFM image (Fig. 2(c)), suggesting the polarization direction of the films on STO (111) is perpendicular to the substrate.

In order to further simplify the domain structure of the BFO films, one must induce a break in symmetry for the ferroelectric variants. One avenue to accomplish this is through the use of vicinal STO substrates, which effectively tilt and break the surface symmetry of the polarization variants [30]. Through the use of a substrate with a vicinal angle along only the [010], the domain structure of the BFO films exhibits mainly two polarization variants. Stripe patterns, created by two polarization variants 71° apart with polarization

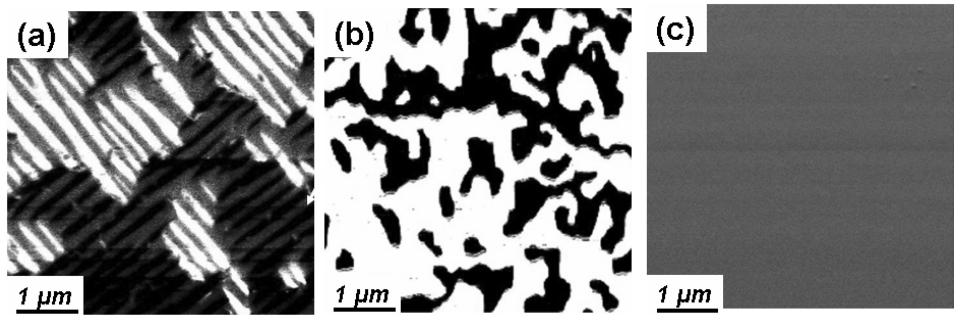

Figure 2. 2 IP-PFM images of BFO ferroelectric domain structures on (a) STO (001), (b) (110), and (c) (111) substrates.

vectors pointing into the substrate, can also be observed. Moreover, by using a substrate with the miscut along the [110], the formation of one dominant ferroelectric variant can be induced. The same approach can be applied to BFO films grown on STO (110). The two-domain architecture in the BFO (110) films can likewise be controlled and evolved into a single domain film on the STO (110) surface. In order to verify the polarization variants, therefore, RSM have been used to further confirm the domain architecture in these samples.

Implementation of this vicinal substrate approach on (100) and (110) STO substrates has given us the ability to create single domain BFO films on such surfaces. This, in conjunction with the fact that epitaxial films on (111) STO with a SRO bottom electrode also exhibit a single domain behavior, provides us with set of model thin film systems to further explore the magnetoelectric properties of this system as well as its interactions with other layers. Additionally, multiferroic and ferroelectric materials with periodic domain structures, like that shown in Fig. 3(b), are of great interest for applications in photonic devices. In recent work, an approach to create a 1-dimensional periodic structure of ferroelectric domains in epitaxial BFO films was demonstrated [35]. The schematic of the constraints imposed by heteroepitaxy to create long range order in the domain structure of BFO was shown in Fig. 3(a). First, we use the fact that on the (110) surface, the DSO lattice is extremely closely matched to that of SRO. Further, the small structural anisotropy in DSO is used to pin the structure of the SRO layer such that a single domain variant of the SRO is formed under the appropriate growth conditions. This structurally simplified SRO film was then used to provide an anisotropic strain to exclude two of the four possible ferroelectric polarization variants and induce a 1-D periodic ferroelectric domain structure in the BFO films.

As we have mentioned previously, control of multiferroic behavior in BFO films relies on being able to control the ferroelectric domain switching. Using PFM, one can identify the different types (71°, 109°, and 180°) of electric field-induced polarization switching mechanisms [36]. To locally switch the films, a DC bias was applied to the conducting atomic force microscope (AFM) tip while scanning over the desired area. By analyzing the

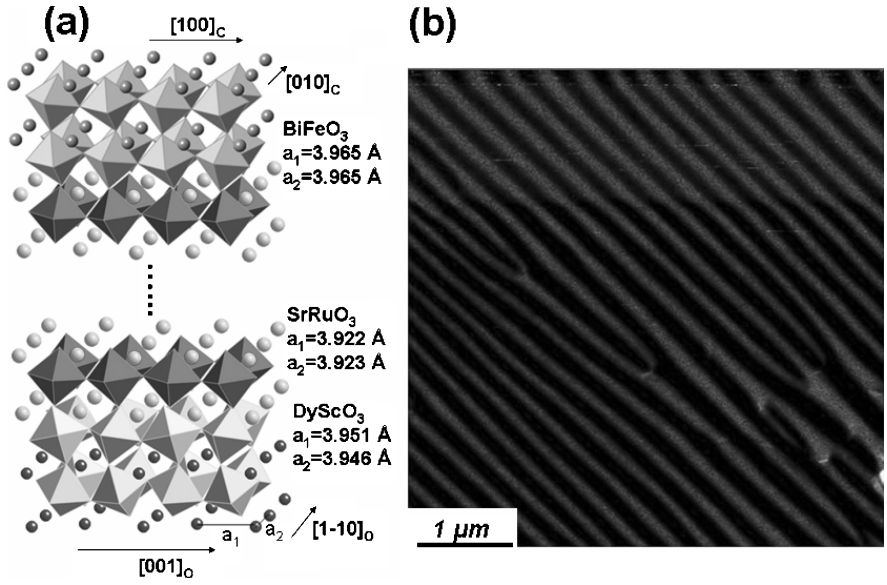

Figure 3. (a) Schematic of the BFO/SRO/DSO heterostructure and (b) IP-PFM images of BFO films with periodic domain structure.

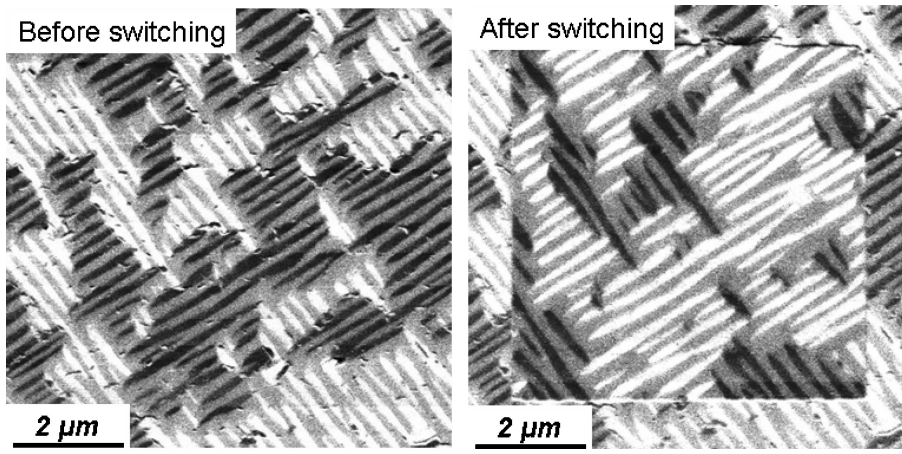

Figure 4. IP-PFM images (001) BFO/SRO/STO films before and after switching.

OP and IP contrast changes following this electrical poling in the epitaxial BFO (001) films, all three possible switching mechanisms have been observed (Fig. 4). In order to control the ferroelectric switching, both a simplified BFO domain structure and the use of varying applied voltages are used to separate the ferroelectric switching and control all three types of switching events in the BFO (110) films [37]. Such results demonstrate the capability to control the multiferroic order in BFO films by exerting precise control over the ferroelectric order parameter.

Finally, the ferroelectric nature of BFO has varied greatly in many recent reports [6, 38]. Trouble with high leakage currents and poor electrical contacts has lead to what may be considered BFO's greatest limiting factor – ferroelectricity. Recently, BFO films on DSO substrates have been shown to have much more ideal ferroelectricity [35]. The macroscopic electrical polarization-field ($P - E$) hysteresis loops with different measuring frequencies of the BFO films are shown in Fig. 5(a). These loops are sharp, square loops and yield a $2P_r$ value of 120 μC/cm^2, which is consistent with first principles calculations [22]. Sharp ferroelectric loops can be obtained even at a low frequency of 200 Hz and leakage measurements

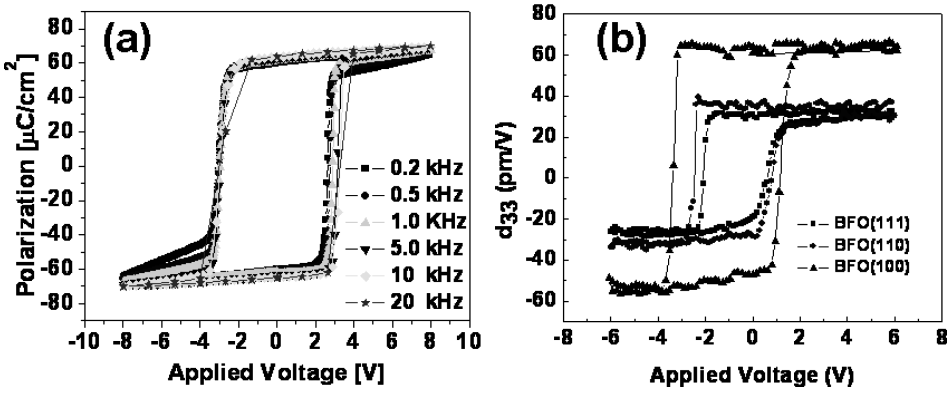

Figure 5. (a) The macroscopic electrical polarization-field (P-E) hysteresis loops with different measuring frequency, and (b) Piezoelectric hystersis loops, $d33 - V$, of BFO/SRO films on different orientation STO substrates.

indicate low leakage levels ($<10^{-7}$ A) at 10 V. To quantitatively measure the piezoelectric response of BFO films, an atomic force microscope-based setup has been employed. The remnant d_{33} value for the fully clamped BFO films increases from 30 pm/V to 60 pm/V for BFO films with different orientation (Fig. 5(b)), as the number of ferroelectric polarization variants is increased. Such an enhancement is attributed to an extrinsic contribution from domain wall motion, which is evident if we compare the domain structure of the BFO films.

III. Future Directions

(1) Improvement in Ferroelectric Properties

As we identified previously, the first major issue to overcome in BFO thin films is leakage. Understanding the leakage source in BFO films is a crucial first step to solve this problem. The literature on possible leakage current limiting mechanisms for ferroelectric perovskite oxides discusses a large number of possible mechanisms [39, 40]. Careful I-V measurements have been carried on SRO/BFO/SRO/DSO (110) structures as a function of the voltage and temperature. Analysis of the electrical response of these films points to Poole-Frenkel emission as the limiting leakage current mechanism in the case of sysmmetric devices structures with heteroepitaxial oxide contacts [41]. Additionally, many researchers and companies are investigating either A- or B-site dopants as a means of lowering leakage currents in BFO based devices [38, 42–44].

The second issue in terms of ferroelectricity that must be addressed is the coercivity. The coercive field of BFO films (250 kV/cm) is significantly higher than the corresponding values for the PZT system. For FeRAM applications, a value around 50–70 kV/cm would be desirable. Furthermore, there has not yet been a direct study aimed at understanding the mechanisms responsible for these large coercive fields. Along these lines, work with La-substitution at the A^{3+}-site in PZT has demonstrated that we can lower the coercivity to levels more consistent with the tetragonal PZT system [24]. Following this logic, rare-earth ion substitutions (La and Nd)on the A-site have been attempted in the past in BFO [45, 46]. Unfortunately, there is yet no effective solution to achieve the low coercivity in BFO.

Finally, in order for BFO to become widely accepted in ferroelectric applications, the reliability issue must also be resolved, including factors such as retention, fatigue and imprint. So far, there has been no focused study on these issues as well. One positive for acceptance of BFO, however, is the integration capability with semiconductors like Si and GaN that has been demonstrated by using a STO template layer [19, 47].

(2) Use of the Magnetoelectric Coupling in BFO

BFO has the remarkable property of simultaneously being a very good ferroelectric and antiferromagnet at room temperature. Recently, what has been seen is the evidence of coupling between the ferroelectric and magnetic order parameters in BFO. As mentioned previously, studies combining PFM and PEEM have enabled researchers to show electrical control of antiferromagnetic domains at room temperature. Such a result provides a great potential to control the magnetism by applying an electric field. The question then posed to researchers is how can we take this one step further? One possible answer is through the use of materials like BFO in exchange bias heterostructures [48, 49]. Exchange bias, or the creation of a unidirectional anisotropy in a ferromagnet through an exchange interaction

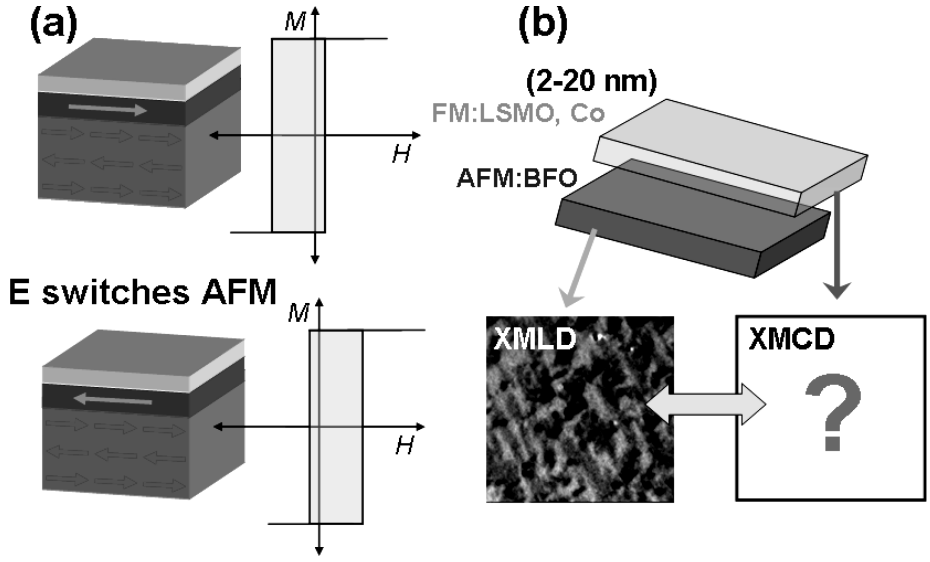

Figure 6. (a) Schematic showing the use of BFO films to control the ferromagnetism via an exchange coupling interaction. (b) PEEM offers an avenue to probe and understand the interaction between the multiferroic BFO and ferromagnetic layer. (See Color Plate VIII)

with an antiferromagnet, has been widely studied. But what will happen when we replace the traditional antiferromagnet with a magnetoelectric, multiferroic? Can we gain electrical control over the exchange bias interaction (Fig. 6(a))? These are the questions that remain to be answered. Therefore, the first step is to prove and understand coupling mechanism in this heterostructure. PEEM measurement is crucial tool to probe this [50]. This technique offers high spatial resolution to antiferromagnetism and ferromagnetism depended on the polarization of the light source. By using this, the relationship of the multiferroic BFO and ferromagnetic layer can be determined (Fig. 6(b)), which will provide the information to demonstrate how to use the electrical field to control magnetism.

IV. Conclusions

In summary, we have reviewed the current status of work concerning the highly precise control of the multiferroic BFO in epitaxial thin films. We have seen how careful consideration in growth can effect immense changes in crystalline structure and domain structure. We have examined how to control the domain structure, the domain switching mechanisms, and the basic ferroelectric properties. Moreover, we addressed several current issues of BFO films, such as coercivity, leakage, process integration. We also proposed some future directions, like application based on ferroelectric properties and exciting possibility of electrically control magnetism.

Acknowledgment

This work was supported by the National Science Foundation under Grant No. EEC-0425914; by the Director, Office of Science, Office of Basic Energy Sciences, Materials Sciences and Engineering Division, of the U.S. Department of Energy under Contract

No. DE-AC02-05CH11231; and by the Office of Naval Research under ONR Grant No. N00014-06-1-0008 and ONR-MURI Grant No. E-21-6RU-G4.

References

1. V. L. Ginzburg, *Soviet Phys.-Solid State* **2**, 1824 (1961)
2. Y. Tokura, *Science* **312**, 1481 (2006).
3. R. Ramesh and N. A. Spaldin, *Nature Mater.* **6**, 21 (2007).
4. W. Eerenstein, N. D. Mathur, and J. F. Scott, *Nature* **442**, 759 (2006).
5. N. A. Spaldin and M. Fiebig, *Science* **309**, 391 (2005).
6. M. Fiebig, Th. Lottermoser, D. Frohlich, A. V. Goltsev, and R. V. Pisarev, *Nature* **419**, 818 (2002).
7. J. Wang, J. B. Neaton, H. Zheng, V. Nagarajan, S. B. Ogale, B. Liu, D. Viehland, V. Vaithyanathan, D. G. Schlom, U. V. Waghmare, N. A. Spaldin, K. M. Rabe, M. Wuttig, and R. Ramesh, *Science* **299**, 1719 (2003).
8. Z. J. Huang, Y. Cao, Y. Y. Sun, Y. Y. Xue, and C. W. Chu, *Phys. Rev. B* **56**, 2623 (1997).
9. N. Hur, S. Park, P. A. Sharma, J. S. Ahn, S. Guha, and S. W. Cheong, *Nature* **429**, 392 (2004).
10. G. Srinivasan, E. T. Rasmussen, B. J. Levin, and R. Hayes, *Phys. Rev. B* **65**, 134402 (2002).
11. H. Zheng, J Wang, S. E. Lofland, Z. Ma, L. Mohaddes-Ardabili, T. Zhao, L. Salamanca-Riba, S. R. Shinde, S. B. Ogale, F. Bai, D. Viehland, Y. Jia, D. G. Schlom, M. Wuttig, A. Roytburd, R. Ramesh, *Science* **303**, 661 (2004).
12. G. A. Smolenskii, V. Isupov, A. Agranovskaya, and N. Kranik, *Sov. Phys. Solid State* **2**, (2), 2651 (1961).
13. P. Fischer, M. Połomska, I. Sosnowska, and M. Szymański, *J. Phys. C* **13**, 1931 (1980).
14. C. Michel, J. M. Moreau, G. D. Achenbechi, R. Gerson, W. J. James, *Solid State Commun.* **7**, 701 (1969).
15. F. Kubel and H. Schmid, *Acta Crystallogr., Sect. B: Struct. Sci.* **B46**, 698 (1990).
16. C. Ederer and N. A. Spaldin, *Phys. Rev. B* **71**, 060401(R) (2005).
17. F. Bai, J. Wang, M. Wuttig, J. Li, N. Wang, A. P. Pyatakov, A. K. Zvezdin, L. E. Cross, and D. Viehland, *Appl. Phys. Lett.* **86**, 032511 (2005).
18. T. Zhao, A. Scholl, F. Zavaliche, K. Lee, M. Barry, A. Doran, M. P. Cruz, Y. H. Chu, C. Ederer, N. A. Spaldin, R. R. Das, D. M. Kim, S. H. Baek, C. B. Eom, and R. Ramesh, *Nature Mater.* **5**, 823 (2006).
19. J. Wang, H. Zheng, Z. Ma, S. Prasertchoung, M. Wuttig, R. Droopad, J. Yu, K. Eisenbeiser, and R. Ramesh, *Appl. Phys. Lett.* **85**, 2574 (2004).
20. S. Y. Yang, F. Zavaliche, L. Mohaddes-Ardabili, V. Vaithyanathan, D. G. Schlom, Y. J. Lee, Y. H. Chu, M. P. Cruz, Q. Zhan, T. Zhao, and R. Ramesh, *Appl. Phys. Lett.* **87**, 102903 (2005).
21. C. Ederer and N. A. Spaldin, *Phys. Rev. B* **71**, 224103 (2005).
22. C. Ederer and N. A. Spaldin, *Phys. Rev. Lett.* **95**, 257601 (2005).
23. H. Bea, M. Bibes, M. Sirena, G. Herranz, K. Bouzehouane, E. Jacquet, S. Fusil, P. Paruch, M. Dawber, J. P. Contour, and A. Barthelemy, *Appl. Phys. Lett.* **88**, 062502 (2006).
24. Y. H. Lee, C. C. Lee, Z. X. Liu, C. S. Liang, and J. M. Wu, *Electrochem. Solid-State Lett.* **8**, F55 (2005).
25. R. R. Das, D. M. Kim, S. H. Baek, F. Zavaliche, S. Y. Yang, X. Ke, S. K. Streiffer, M. S. Rzchowski, R. Ramesh, and C. B. Eom, *Appl. Phys. Lett.* **88**, 242904 (2006).
26. R. Ueno, S. Okaura, H. Funakubo, and K. Saito, *Jpn. J. Appl. Phys.* **44**, L1231 (2005).
27. S. K. Singh, Y. K. Kim, H. Funakubo, and H. Ishiwara, *Appl. Phys. Lett.* **88**, 162904 (2006).
28. G. Xu, H. Hiraka, G. Shirane, J. F. Li, J. Wang, and D. Viehland, *Appl. Phys. Lett.* **86**, 182905 (2005).
29. G. Xu, J. Li, and D. Viehland, *Appl. Phys. Lett.* **89**, 222901 (2006).
30. Y. H. Chu, M. P. Cruz, C. H. Yang, L. W. Martin, P. L. Yang, J. X. Zhang, K. Lee, P. Yu, L. Q. Chen, and R. Ramesh, *Adv. Mater.* in print (2007).

31. J. X. Zhang, Y. L. Li, S. Choudhury, Y. H. Chu, F. Zavaliche, Q. X. Jia, D. G. Schlom, R. Ramesh, and L. Q. Chen, *J. Appl. Phys.* submitted (2007).
32. L. Q. Chen, *Ann. Rev. Mater. Res.* **32**, 113 (2002).
33. S. K. Streiffer, C. B. Parker, A. E. Romanov, M. J. Lefevre, L. Zhao, J. S. Speck, W. Pompe, C. M. Foster, and G. R. Bai, *J. Appl. Phys.* **83**, 2742 (1998).
34. F. Zavaliche, R. R. Das, D. M. Kim, S. Y. Yang, P. Shafer, C. B. Eom, and R. Ramesh, *Appl. Phys. Lett.* **87**, 182912 (2005).
35. Y. H. Chu, Q. Zhan, L. W. Martin, M. P. Cruz, P. L. Yang, G. W. Pabst, F. Zavaliche, S. Y. Yang, J. X. Zhang, L. Q. Chen, D. G. Schlom, I. Nan. Lin, T. B. Wu, and R. Ramesh, *Adv. Mater.* **18**, 2307 (2006).
36. F. Zavaliche, P. Shafer, M. P. Cruz, R. R. Das, D. M. Kim, C. B. Eom, and R. Ramesh, *Appl. Phys. Lett.* **87**, 252902 (2005).
37. M. P. Cruz, Y. H. Chu, J. X. Zhang, F. Zavaliche, P. L. Yang, P. Shafer, L. Q. Chen, and R. Ramesh, to be submitted (2007).
38. X. Qi, J. Dho, R. Tomov, M. G. Blamire, and J. L. MacManus-Driscoll, *Appl. Phys. Lett.* **86**, 062903 (2005).
39. B. Nagaraj, S. Aggarwal, T. K. Song, T. Sawhney, and R. Ramesh, *Phys. Rev. B* **59**, 16022 (1999).
40. P. Zubko, D. J. Jung, and J. F. Scott, *J. Appl. Phys.* **100**, 114113 (2006).
41. G. W. Pabst, L. W. Martin, Y. H. Chu, and R. Ramesh, *Appl. Phys. Lett.* 072902 (2007).
42. C. F. Chung, J. P. Lin, and J. M. Wu, *Appl. Phys. Lett.* **88**, 242909 (2006).
43. Y. Wang and C. W. Nan, *Appl. Phys. Lett.* **89**, 052903 (2006).
44. S. R. Shannigrahi, A. Huang, N. Chandrasekhar, D. Tripathy, and A. O. Adeyeye, *Appl. Phys. Lett.* **90**, 022901 (2007).
45. H. Uchida, R. Ueno, H. Funakubo, and S. Koda, *J. Appl. Phys.* **100**, 014106 (2006).
46. G. L. Yuan, S. W. Or, H. L. W. Chan, and Z. G. Liu, *J. Appl. Phys.* **101**, 024106 (2006).
47. W. Tian, V. Vaithyanathan, D. G. Schlom, Q. Zhan, S. Y. Yang, Y. H. Chu, and R. Ramesh, *Appl. Phys. Lett.* 172908 (2007).
48. J. H. Dho, X. D. Qi, H. Kim, J. L. MacManus-Driscoll, and M. G. Blamire, *Adv. Mater.* **18**, 1445 (2006).
49. H. Bea, M. Bibes, S. Cherifi, F. Nolting, B. Warot-Fonrose, S. Fusil, G. Herranz, C. Deranlot, E. Jacquet, K. Bouzehouane, and A. Barthelemy, *Appl. Phys. Lett.* **89**, 242114 (2005).
50. F. Nolting, A. Scholl, J. Stöhr, J. W. Seo, J. Fompeyrine, H. Siegwart, J.-P. Locquet, S. Anders, J. Lüning, E. E. Fullerton, M. F. Toney, M. R. Scheinfein, and H. A. Padmore, *Nature* **405**, 767 (2000).